Atmos. Chem. Phys. Discuss., 15, 29705–29745, 2015
www.atmos-chem-phys-discuss.net/15/29705/2015/
doi:10.5194/acpd-15-29705-2015

Atmospheric Chemistry and Physics Discussions

Sensitivity of modeled atmospheric nitrogen species to variations in sea salt emissions in the North and Baltic Sea regions

D. Neumann, V. Matthias, J. Bieser, A. Aulinger, and M. Quante

Helmholtz-Zentrum Geesthacht, Institute of Coastal Research, Max-Planck-Straße 1, 21502 Geesthacht, Germany

Received: 25 September 2015 – Accepted: 16 October 2015 – Published: 30 October 2015

Correspondence to: D. Neumann (daniel.neumann@hzg.de)

Published by Copernicus Publications on behalf of the European Geosciences Union.

Abstract

Coarse sea salt particles are emitted ubiquitously from the oceans' surfaces by wave breaking and bubble bursting processes. These particles impact atmospheric chemistry by affecting condensation of gas-phase species and nucleation of new fine particles, particularly in regions with high air pollution. In this study, atmospheric particle concentrations are modeled for the North and Baltic Sea regions, Northwestern Europe, using the Community Multiscale Air Quality (CMAQ) modeling system and evaluated against European Monitoring and Evaluation Programme (EMEP) measurement data. As model extension, sea salt emissions are scaled by water salinity because of low salinity in large parts of the Baltic Sea and in certain river estuaries. The resulting improvement in predicted sea salt concentrations is assessed. The contribution of surf zone emissions is separately considered. Additionally, the impact of sea salt particles on atmospheric nitrate, ammonium and sulfate concentrations is evaluated.

The comparisons show that sea salt concentrations are commonly overestimated at coastal stations and partly underestimated when going inland. The introduced salinity scaling improves predicted Baltic Sea sea salt concentrations considerably. Dates of measured peak concentrations are appropriately reproduced by the model. The impact of surf zone emissions is negligible in both seas. Nevertheless, they might be relevant because surf zone emissions were cut at an upper threshold in this study. Deactivating sea salt leads to a minor increase of NH_4^+ and NO_3^- and a minor decrease of SO_4^{2-} concentrations. However, the overall effect is very low and lower than the deviation from measurements. Size resolved measurements of Na^+, NH_4^+, NO_3^-, and SO_4^{2-} are needed for a more detailed analysis on the impact of sea salt particles.

ACPD
15, 29705–29745, 2015

1 Introduction

Atmospheric sea salt particles are generated from saline water droplets emitted from the sea surface by wind-governed processes and the breaking of waves. Sea salt particle generation is influenced by sea surface temperature, salinity and the composition of the sea surface micro-layer (Martensson et al., 2003; Jaeglé et al., 2011; Gantt et al., 2011). It is considerably enhanced in the surf zone, where waves break along the coast.

Sea salt particles affect the abundance and chemistry of atmospheric pollutants in various ways. Gas-phase species condense on coarse sea salt particles instead of nucleating as new ones, and undergo heterogeneous reactions on the particle surfaces (Seinfeld and Pandis, 2006, Chp. 10.4.4 and 10.4.6). Coarse particles have higher dry deposition velocities than fine particles, which leads to faster dry deposition of those species adhering to the course particles. Additionally, hydrochloric acid (HCl) is released from sea salt particles, which affects ozone chemistry in polluted marine air (Cai et al., 2008; Crisp et al., 2014; Knipping and Dabdub, 2003). The effect of sea salt particles on atmospheric chemistry is most relevant in coastal regions where anthropogenic and natural land-emitted species and sea salt particles coincide.

The North and Baltic Sea regions are areas of high anthropogenic activity, including heavy industry, shipping, road transport, agriculture, power generation and residential heating. These activities emit various air pollutants, such as NO_x, SO_2, NH_3 and particulate matter. Although emissions have been reduced over the past 30 years (Lövblad et al., 2004; Crippa et al., 2015), their effects on human health and their environmental impact are still significant. In this air pollution regime, sea salt is expected to play an important role in affecting the deposition and heterogeneous chemistry of relevant pollutants. The target of this study was to evaluate the following questions for the central European domain using the EPA's Community Multiscale Air Quality (CMAQ) modeling system:

a. What effects do sea salt emissions have on atmospheric ammonium and nitrate concentrations?

ACPD
15, 29705–29745, 2015

b. How strongly do surf zone emissions contribute to total sea salt and what influence do these emissions have on (a)?

c. Are sea salt emissions well represented in CMAQ for this region?

These analyses were conducted by setting up three sea salt emission cases and comparing the model results to each other and to European Measurement and Evaluation Program (EMEP) measurement data. Manders et al. (2010) recently evaluated sea salt measurements from various EMEP stations. Modeling air quality in the Eastern Mediterranean Sea using CMAQ, Im (2013) found a strong impact of sea salt emissions on atmospheric nitrate concentrations and considered surf zone emissions to be important. Liu et al. (2015) found a strong impact of sea salt particles on nitrate as well in a modeling study in the Pearl River Delta, China.

In models, sea salt emissions are parameterized by wind speed and other meteorological and oceanic parameters. Several current parameterizations are based on the wind dependence derived by Monahan and Muircheartaigh (1980) and Monahan et al. (1986). Spada et al. (2013) provided a useful overview and comparison of available sea salt emission parameterizations. Additionally, Jaeglé et al. (2011) and Ovadnevaite et al. (2014) recently published improved approaches that include wind speed, salinity, SST, and wave data. However, sea salt emissions are still not well parameterized in the surf zone, an area of increased wave breaking along the coastline. CMAQ employs a parameterization published by Gong (2003) that expands the Monahan et al. (1986) parameterization to smaller particle diameters. This study adds a dependence on salinity.

ACPD
15, 29705–29745, 2015

2 Materials and methods

2.1 Target region

The study region is located in the northeast corner of the Atlantic Ocean and includes the North and Baltic Seas. The North Sea is directly connected to the Atlantic Ocean via the English Channel to the southwest and via the Norwegian Sea to the north. The English Channel is a region of major shipping activity because nearly all ships traveling from outer Europe to the large North European ports, such as Antwerp, Rotterdam and Hamburg, pass through it. In addition to shipping, considerable anthropogenic activity occurs on land, such as industry, agriculture and road traffic. The North Sea has a salinity of approximately 35 ‰, which is similar to the Atlantic Ocean. The Baltic Sea is connected to the North Sea via a natural passage between Denmark and Norway/Sweden. In the Baltic Sea, the salinity is approximately 20 ‰ in the western parts and decreases to below 8 ‰ in the eastern parts. During winter, northeastern parts of the Baltic Sea are covered by sea ice. High anthropogenic activity also occurs on the land and water. However, shipping activity is not as pronounced as in the North Sea.

2.2 Model set up

The simulations were performed with the Community Multi-scale Air Quality (CMAQ) modeling system, which was developed and maintained by the US EPA. Version 5.0.1 was used for this study. The cb05tucl mechanisms, i.e., the Carbon Bond 05 mechanism Yarwood et al. (2005) with updated toluene (Whitten et al., 2010) and chlorine chemistry (Tanaka et al., 2003; Sarwar et al., 2007), represented the gas phase chemistry. Heterogeneous chemistry is covered by the AERO05 mechanism, which is based on the ISORROPIA2 (Fountoukis and Nenes, 2007) mechanism. Among other processes, this mechanism governs the condensation of HCl, NH_3, HNO_3 and H_2SO_4 on particles and the nucleation of new particles. HCl, NH_3 and HNO_3 may evaporate back into the gas phase, whereas H_2SO_4 does not. The aerosol phase is

ACPD
15, 29705–29745, 2015

modeled by three lognormal-distributed modes that are each represented by three moments (Binkowski and Roselle, 2003). The AERO05 mechanism is described in the CMAQ Wiki (http://www.airqualitymodeling.org/cmaqwiki). CMAQ also includes in-cloud chemistry.

The study region is covered by a grid of 24 km × 24 km resolution and is enclosed by a grid of 72 km × 72 km resolution covering Europe (Fig. 1). The boundary conditions of the outer grid are taken from monthly means of the tM5 global chemistry transport model system (Huijnen et al., 2010), and the boundary conditions of the 24 km grid are taken from the enclosing 72 km grid. Wind-blown dust is not included in the outer boundary conditions.

Two three-month periods – January to February and July to August 2008 – denoted as winter and summer, respectively, are considered. No model input data for December 2007 and no German EMEP measurement data for September to December 2008 were available. Therefore, it was decided to represent winter and summer by two months each. A 10 day spin-up phase, which was initiated from standardized spatially homogeneous initial conditions, preceded each of the two periods.

2.3 Input data

Meteorological input data were calculated by COSMO-CLM (Consortium for Small-scale Modeling in Climate Mode) version 4.8 on a rotated lon-lat grid of 0.22° resolution with hourly output (Geyer and Rockel, 2013; Geyer, 2014). The model grid covers Europe, parts of Greenland and the southern coast of the Mediterranean Sea. The data were remapped onto the CMAQ grid, and relevant variables were extracted and converted using a modified version of CMAQ's Meteorology-Chemistry Interface Processor (MCIP) (Otte and Pleim, 2010).

The European land-based emissions were compiled with SMOKE for Europe (Bieser et al., 2011), and agricultural emissions were updated according to Backes et al. (2015a, b). Shipping emissions were calculated on the basis of Automated Identifi-

ACPD
15, 29705–29745, 2015

cation System (AIS) data (Aulinger et al., 2015). Sea salt emissions were calculated inline (Kelly et al., 2010; Gong, 2003). Details are given in the next section.

2.4 Sea salt emissions

Physically, sea salt particles are dried sea water droplets that are ejected from the sea surface into the atmosphere (Lewis and Schwartz, 2004). Under most weather conditions, the generation of sea salt particles is dominated by bubble bursting: air is mixed into sea water by breaking waves and forms air bubbles that rise to the sea surface and burst. Small water droplets are ejected from the breaking hull of the bubble (film droplets). Through the abruptly changing pressure within the bursting bubble, some water is sucked from below the bubble into the air (jet droplets). The fraction of sea surface covered by bursting bubbles is denoted as white cap coverage. Droplets, which are emitted primarily when waves break and which are torn by the wind from wave crests, are denoted as spume and splash droplets, respectively. High wind speeds of approximately larger than $10\,m\,s^{-1}$ are needed for both processes to be relevant for atmospheric sea salt particle generation. The naming conventions for spume and splash droplets are not consistent throughout the literature.

The amount of sea salt per droplet and the resulting sea salt particle size are governed by the sea surface salinity (Martensson et al., 2003). Sea surface temperature, biofilms and other surfactants affect the sea salt particle size spectra (Martensson et al., 2003; Gantt et al., 2011). In the surf zone, sea salt emissions are enhanced due to a higher number of breaking waves. Additionally, sea salt particles may be electrically charged (Gathman and Hoppel, 1970; Bowyer et al., 1990).

2.4.1 Sea salt emission parameterizations in CMAQ

Edward Monahan and colleagues (Monahan et al., 1982; Monahan and Muircheartaigh, 1980) derived a parameterization that describes the generation of sea salt particles by bursting bubbles. A sea salt particle number flux distribution was estimated

ACPD
15, 29705–29745, 2015

for 100 % white cap coverage and multiplied by the white cap coverage W, which is fitted by a power law to the 10 m wind speed (u_{10}) as given in Eq. (1) (Monahan et al., 1986, Eq. 12). Sea salt emissions in CMAQ are calculated following Gong (2003), an enhancement of Monahan et al. (1982) that incorporates smaller radii (see Eq. 2). Particle number, dry surface, dry mass flux and water content at an ambient relative humidity (RH) are calculated explicitly in CMAQ. Water content is calculated using a polynomial fit published by Zhang et al. (2005). The total emitted dry sea salt mass is split into 7.55 % SO_4^{2-}, 53.98 % Cl^-, and 38.56 % Na^+ (Kelly et al., 2010). The model Na^+ represents Na^+, Mg^{2+}, K^+, and Ca^{2+}.

$$W = 3.84 \times 10^{-6} \times u_{10}^{3.41} \tag{1}$$

$$\frac{dF}{dr_{80}} = W \times 3.5755 \times 10^5 \times r_{80}^{-A} \times \left(1 + 0.057 \times r_{80}^{3.45}\right) \times 10^{1.607 \times e^{-B^2}}$$

$$= 1.373 \times u_{10}^{3.41} \times r_{80}^{-A} \times \left(1 + 0.057 \times r_{80}^{3.45}\right) \times 10^{1.607 \times e^{-B^2}} \tag{2}$$

$$A = 4.7 \times (1 + \theta \times r_{80})^{-0.017 \times r_{80}^{-1.44}}$$

$$B = \frac{0.433 - \log(r_{80})}{0.433}$$

In the above equations, r_{80} [µm] is the particle radius at 80 % relative humidity, u_{10} [m s^{-1}] is the 10 m wind speed and θ is an adjustable parameter, which is set to 30. The term dF/dr is the number flux [number m^{-2} µm^{-1} s^{-1}] of sea salt particles. The parameterization is valid in a size range of 0.06 µm $\leq r_{80} \leq$ 20 µm.

2.4.2 Surf zone emissions

In the surf zone, the sea salt particle number flux is considerably higher than in the open ocean. Addressing surf zone emissions is quite difficult because they depend on the direction of waves and the wind, as well as on local coastal features, such as steep

ACPD
15, 29705–29745, 2015

cliffy coasts and flat beaches. In the employed CMAQ version, the surf zone is parameterized by setting the white cap coverage W to 1. The surf zone area is proposed to be a 50 m wide strip along the coastline (Kelly et al., 2010). CMAQ simulations in parts of Florida performed well with this definition of surf zone (J. T. Kelly, personal communication, 2014). Equation (3) shows a modified emission function in-cooperating surf zone and open ocean fractions. These fractions need to be pre-calculated for each model domain.

$$\frac{dF_{eff}}{dr_{80}} = (W \times \text{open} + \text{surf}) \times \frac{1}{W} \times \frac{dF}{dr_{80}} \quad (3)$$

For this study, the ratios of open ocean and surf zone surface per grid cell were calculated by ArcGIS based on the Natural Earth data set: the surf zone area was obtained by placing a 50 m wide strip along the coastline and calculating the area of that strip. Overlapping areas were ignored. Grid cells with long fragmented coastlines and many islands do not necessarily have a large surf zone area because some parts of the coastline and islands are protected by others. Therefore, the surf zone fraction per grid cell was cut at a threshold (see Supplement for details).

2.4.3 Salinity dependence

The salinity in large parts of the Baltic Sea is less than 10 ‰ , in contrast to the North Sea's 35 ‰. Therefore, the sea salt emissions must be corrected to account for differences in salinity. The open ocean and surf data were scaled by the salinity S (S/0.035, with 0.035 = 35 ‰) to obtain salinity-dependent sea salt emissions (Martensson et al., 2003). CMAQ sea salt emissions would otherwise not depend on salinity. Sea ice cover is not considered. Finally, Eq. (4) for sea salt emissions was obtained:

$$\frac{dF_{eff}}{dr_{80}} = \frac{S}{0.035} \times (W \times \text{open} + \text{surf}) \times \frac{1}{W} \times \frac{dF}{dr_{80}} \quad (4)$$

The technical procedure of including salinity dependence is described in the Supplement Sect. A.

ACPD
15, 29705–29745, 2015

2.4.4 Sea salt emission scenarios

Three different sea salt emission cases are investigated in this study: base, noSurf and zero. The base case corresponds to the standard CMAQ sea salt emissions. The zero case contains no sea salt emissions. In the noSurf case, the surf zone is treated as the open ocean. The cases are listed in Table 1.

2.5 Evaluation procedure

The CMAQ simulation results were evaluated against concentration measurements performed at EMEP stations. The data were obtained via EBAS (http://ebas.nilu.no/). The stations were chosen according to the availability of data for comparison (Fig. 2). Three stations – Westerland (DE0001R), Waldhof (DE0002R), and Zingst (DE0009R) – are described in detail in Sect. 3; the data from the other stations are included in the Supplement. The Westerland station is located directly on the North Sea coast, Zingst is located on the Baltic Sea coast, and Waldhof is located approximately 200 km inland.

Species including Na^+, corrected SO_4^{2-}, $NH_3 + NH_4^+$ and $HNO_3 + NO_3^-$ were compared. Sodium cations (Na^+) represent pure sea salt. They are considered for evaluating sea salt particle predictions. Corrected sulfate, xSO_4, is defined as total sulfate minus sea salt sulfate. Because natural sulfate sources such as DMS are quite low, xSO_4 commonly represents anthropogenically emitted sulfate. Ammonium (NH_4^+) and ammonia (NH_3) as well as nitrate (NO_3^-) and nitric acid (HNO_3) are considered as sums only. Because these substances are collected with three filter packs at certain EMEP stations, the individual measurements of NH_4^+, NH_3, NO_3^-, and HNO_3 are subject to large uncertainties, whereas the sums are accurately determined (EMEP, 2014, Chp. 3).

Daily mean concentrations are compared as plotted time series, box plots, and via three statistical metrics: mean normalized bias (MNB), residual absolute error (RAE), and Spearman's correlation coefficient (R). See Schlünzen and Sokhi (2008) for de-

ACPD
15, 29705–29745, 2015

scriptions of these figures. The box plots contain data of only those days for which measurement data are available.

3 Results

3.1 Emissions

Figure 3 shows modeled monthly averaged sea salt emissions for the base emission case (top row) in winter and summer (left and right columns, respectively). The bottom row shows differences between noSurf and base cases.

According to Fig. 3, winter sea salt emissions are two to five times higher than summer sea salt emissions due to higher wind speeds. In the Baltic Sea, sea salt emissions are considerably lower than in the North Sea, which is caused by the salinity-dependent downscaling of the sea salt emissions. Because wind speeds decrease towards the coast and are highest above open waters, sea salt emissions decrease towards the coast as well. Comparing the base and noSurf sea salt emissions, the greatest differences are observed along the Norwegian and British Atlantic coasts, and lowest differences are observed along the Baltic Sea coast.

Figure 4 shows daily averaged sea salt emissions in three coastal grid cells. Although the surf zone covers only a small fraction of the grid cell surface, surf zone emissions contribute a considerable share of sea salt emissions in low wind speed situations. This result emphasizes the importance of correctly parameterizing surf zone sea salt emissions.

3.2 Concentrations

Modeled and measured concentrations of two 90 day time series at three EMEP stations, i.e., Westerland (DE0001R), Waldhof (DE0002R), and Zingst (DE0009R), are described and discussed in this section. For each species and station, the actual time series, box plots of the data and statistical key figures are presented. For the box plots,

ACPD
15, 29705–29745, 2015

only the modeling data points that had corresponding measurement data points were used. The corresponding raw and statistical data from the remaining 12 stations are attached as Supplement.

3.2.1 Sodium

The concentration time series in Fig. 5 shows that the dates of peaks are consistent across all three stations. The correlation coefficient is greater than 0.75 in winter and greater than 0.70 in summer. However, the magnitudes of the peak values do differ in most situations. The model overestimates these values. During winter, overestimations of peak concentrations occur at all stations, which is indicated by the box plots (Fig. 5) and the bias values (Table 2). During summer, sea salt is moderately overestimated at coastal stations (Westerland and Zingst) and underestimated inland (Waldhof), as indicated by the bias values. The measured base line concentrations, i.e., when no peaks are present, are well matched by the model. Winter sodium concentrations are approximately twice as high as summer concentrations (see scale in Fig. 5).

Surf zone emissions lead to a reduction in the modeled concentrations most of the time. MNB is reduced at all stations. This reduction leads to an improved bias in overestimation situations. Surf zone emissions have an important impact in certain low-emission periods, such as in mid-February and at the end of July, when surf zone emissions contribute more than the half of the atmospheric sodium. The zero case is not considered here. The orange line represents a simulation without salinity-dependent scaling of sea salt emissions. The simulation considerably overestimated sodium concentrations at Zingst (Baltic Sea coast). Salinity scaling of emissions is therefore important. Because sodium concentrations are not underestimated at Zingst and not as overestimated as in the non-salinity-scaling case, we assume that the applied linear salinity scaling of the sea salt emissions in the Baltic Sea is a valid procedure as a first-order correction.

ACPD
15, 29705–29745, 2015

3.2.2 Corrected sulfate

The temporal occurrence of peak concentrations is well represented by the modeled corrected SO_4^{2-} (xSO_4) concentrations in Fig. 6. The correlation coefficients are greater than 0.6, except for Waldhof in winter (0.57). Generally, winter peak concentrations are underestimated, particularly in late February, but the background concentrations at Westerland and Zingst are slightly overestimated, as indicated by the MNB. Summer peak concentrations are better matched than the winter peak concentrations. Baseline concentrations are partly over- and partly underestimated.

The sea salt emission time series plots of the base and noSurf case do not show any relevant differences. The *R*, MNB, and RAE values confirm this observation. Deactivating sea salt emissions leads to a slight reduction in xSO_4 peak concentrations in a few situations.

3.2.3 Ammonia and ammonium

$NH_3 + NH_4^+$ (sNH_4, s = sum) concentrations are slightly underestimated at Westerland, as shown in the time series (Fig. 7) and indicated by the box plots and the MNB (Table 4). During summer, the absolute MNB value is high, but the correlation is strong, which can also be seen directly in the time series in Fig. 7: the shape is well matched, but the predicted magnitude is generally too low. In winter, certain peak concentrations are overestimated, which improves the MNB and RAE values, but decreases R. At Waldhof, baseline concentrations are well matched, but peak concentrations are overestimated. In winter, the MNB is lower than during summer due to a strongly underestimated time period at the end of February. The correlation coefficient is 0.59 in winter and increases slightly in summer to 0.63. At Zingst, the measured concentrations are most consistent in terms of the order of magnitude, which is represented by MNB ≈ 0 and by a low RAE. The occurrence of peaks is well matched, but the correlation coefficient is below 0.5 in summer. This pattern is caused by peak concentrations that are sometimes over- and sometimes underestimated. For example, in late July,

ACPD
15, 29705–29745, 2015

CMAQ predicts a decrease in concentrations, but measured concentrations increase. This episode will be analyzed in more detail in Sect. 4.3.

The effect of surf zone sea salt emissions is negligible, as indicated by the plots and statistics. During winter, zero case sNH_4 concentrations increase slightly, particularly when peak concentrations occur. Because these peak concentrations are already overestimated in the base case, deactivating sea salt emissions decreases the prediction quality.

3.2.4 Nitrate and nitric acid

When analyzing $HNO_3 + NO_3^-$ (sNO_3, s = sum) concentrations, one has to distinguish between Westerland on one side and Waldhof and Zingst on the other side. At Westerland, several measured concentrations in the EMEP database are marked as "under detection limit", which leaves only 21 comparable values in winter and 26 in summer. In mid-February, very high concentrations are predicted, even though the measured values were below the detection limit. Due to the low number of valid measurements, Westerland was not analyzed further.

At Waldhof, the average concentrations are well represented, as indicated by box plots (Fig. 8) and MNB (Table 5). In winter, the timing of peaks is well matched, but their heights are overestimated in some situations and underestimated in others. This leads to a high RAE value of approximately 0.6. Additionally, in mid-February, one wide and high peak is considerably overestimated. In summer, the RAE improves. However, the correlation coefficient decreases from 0.64 to 0.34 due to two quite poorly matched peaks at the beginning and end of August. The winter concentrations at Zingst are very well represented by CMAQ. The time series plots and box plots agree with each other, yielding an R value of 0.76. In summer, the correlation decreases. A period of highly underestimated sNO_3 concentrations exists in late July at Zingst and Waldhof.

In the no surf zone case, sNO_3 concentrations are slightly higher than those of the base case. Deactivating sea salt emissions generally increases predicted sNO_3 concentrations. The prediction quality, i.e., R and MNB, increases at Waldhof and Zingst

ACPD
15, 29705–29745, 2015

because slightly underestimated concentrations are increased, which automatically improves MNB.

4 Discussion

4.1 Salinity dependence and particle size spectra

The salinity dependence of sea salt emissions was analyzed by Martensson et al. (2003) in laboratory studies. They found that for particles below 0.1 µm dry radius, the number flux remains roughly unchanged, but the number flux distribution was shifted to smaller radii by a factor of $(S/0.035)^{1/3}$ (Martensson et al., 2003, Fig. 5). Thus, the volume flux is reduced by $S/0.035$ and the surface flux by $(S/0.035)^{2/3}$. For particles larger than 0.1 µm (dry radius), they found that the number flux was reduced by an order of magnitude. In the approach chosen in this study, the number, surface, and volume fluxes are all scaled by $S/0.035$. Technically, this process was performed by scaling the fractions of the open ocean and surf zone in one input file by $S/0.035$. The resulting salinity dependence is not in accordance with the findings of Martensson et al. (2003), neither in terms of the fine particles nor the coarse ones. However, this method was the only way to include basic salinity dependence without modifying the CMAQ code. Thus, the chosen solution is easily applicable to other CMAQ versions and by other CMAQ users. Changing the CMAQ code would have meant that the changes needed to be applied in each new CMAQ version.

Two different sea salt fluxes exist: the sea salt surface flux and the effective sea salt flux. The effective sea salt flux represents the sea salt particles emitted from the sea surface that do not fall back into the ocean immediately. The surface flux represents all particles emitted from the sea surface. The effective flux is a combination of the surface flux and the atmospheric behavior of the sea salt particles which means surface emissions flux minus instant dry deposition. Martensson et al. (2003) measured the

ACPD
15, 29705–29745, 2015

surface flux, whereas Gong (2003) described the effective flux. The shift in the number flux distribution of particles less than 1 µm in size due to salinity variations, which Martensson et al. (2003) observed, might not be directly applicable to the effective flux. The shape of the distribution might change as well. Changes in the relative humidity might alter the particle size distribution, as well. Additionally, de Leeuw et al. (2000, Sect. 6) noted that the bubble-bursting process itself might be affected by low-salinity conditions. Therefore, scaling bulk sea salt emissions by functions dependent upon salinity and relative humidity is not necessarily a correct approach. Changes in the distribution's shape need to be evaluated in the laboratory and in real world studies.

4.2 Discussion of the sea salt results

The sodium concentrations were well matched in terms of the order of magnitude and the temporal occurrence of peaks. Measurements at Zingst showed that sea salt emissions were considerably overestimated in this region if salinity scaling was not applied. Therefore, salinity downscaling is important. Further studies should investigate whether an improved downscaling procedure (see Sect. 4.1) improves predicted sea salt concentrations.

Sea salt concentrations tend to be over-predicted at coastal stations (Westerland more so than Zingst) and under-predicted at inland stations (Waldhof). This pattern may be due to a combination of over-predicted sea salt emissions and over-predicted dry deposition velocities for coarse sea salt particles. Additionally, certain peaks are better matched in terms of magnitude than others. This difference may be attributable to meteorological conditions, droplet generation processes missing from Gong's sea salt emission parameterization, and the sea surface micro layer (SML). Because Gong's parameterization lacks splash and spume droplet generation as well as non-wind-related bubble bursting, repeating the simulations with other sea salt emissions parameterizations might yield interesting results. To analyze the impact of the SML, satellite-derived chlorophyll *a* data could be correlated with the deviations between the measured and

ACPD
15, 29705–29745, 2015

modeled results. However, chlorophyll *a* data may not be the ideal proxy (Fuentes et al., 2010).

Under low wind conditions, surf zone emissions are a major source of atmospheric sea salt in the coastal grid cells. The contribution of these emissions decreases under high wind conditions. In this study, the maximum fraction of surf zone per grid cell (24 km × 24 km grid) was capped at 0.47 % to reduce the amount of surf zone emissions. Commonly, this parameter is not capped. Without capping, the fraction of surf zone was greater than 10 % in certain coastal grid cells, particularly along the Norwegian Atlantic coast, with its numerous fjords and islands. Not capping the surf zone would have led to considerably higher surf zone emissions. de Leeuw et al. (2000) found through measurements at a beach in late January that surf zone emissions can contribute approximately 10 times more to ambient atmospheric sea salt concentrations than open ocean emissions. However, at other times, surf zones contribute just 0.1 times as much as the open ocean. The surf zone emissions in grid cells with a large proportion of surf zone, without capping, might be comparable to the maximum-contribution situations observed in de Leeuw et al. (2000). However, the observed high contributions did not occur continuously. Additionally, the measurements were collected in January, when winds are stronger than those in summer. Therefore, the modeled surf zone emissions were reduced by capping the surf zone fraction. Mechanistically, modifying the white cap coverage would have been more correct. In the new CMAQ v5.1 release, surf zone emissions will be reduced by 50 % by setting the white cap coverage to 0.5. This step was not included in this study because changes in the CMAQ code were avoided in order to make the chosen procedure simpler and more applicable in other CMAQ versions. As an alternative, one might choose another parameterization. For example, de Leeuw et al. (2000) and Chomka and Petelski (1997) presented alternative surf zone emission parameterizations. In their study, de Leeuw et al. (2000) analyzed measured surf zone-related sea salt concentrations, meteorological data and video data of the surf zone. They found no correlation between surf zone width or wave height and the surf zone production of sea salt.

ACPD
15, 29705–29745, 2015

Im (2013) estimated a considerably higher contribution of surf zone emissions to atmospheric sea salt concentrations. In that study, the surf zone fraction per grid cell was not capped and was calculated by multiplying the length of the coastlines by 50 m (and dividing by grid cell area). In our study, the surf zone size was calculated in a way so as to not count overlapping surf zones twice. Therefore, the surf zone contribution estimated in this study is lower.

Salinity in coastal waters is commonly lower than in open ocean waters due to freshwater inflow. Thus, surf zone emissions are indirectly scaled down in this study. Im (2013); Kelly et al. (2010, 2014) do not consider salinity. Hence, this study's surf zone emissions are reduced compared to those in the named studies due to salinity dependent scaling.

Sea ice is not considered in this study. If the sea surface is covered with sea ice, no sea salt particles are emitted by bursting bubbles. Therefore, sea salt emissions can be deactivated in regions with sea ice cover. For the study region, sea surface salinity is very low in areas with significant sea ice cover (northeastern Baltic Sea). Additionally, these areas are commonly in the downwind direction to the considered EMEP stations. Therefore, the overestimation of sea salt emissions introduced by not considering sea ice is expected to be negligible. Moreover, sea salt particles have been found to be re-emitted by wind-blown snow from sea ice (Tian-Kunze et al., 2009; Yang et al., 2008). Additionally, the edges of sea ice required a similar treatment as the surf zone. Therefore, deactivating sea salt emissions above sea ice would not necessarily improve sea salt emission prediction quality.

4.3 Discussion of nitrogen and sulfur compounds

The concentrations of sNH_4 were found to be well matched at Zingst, under-predicted at Westerland, and over-predicted at Waldhof. Because land-based NH_3 emissions are not the topic of this paper, Waldhof will not be discussed further. Backes et al. (2015a) described and discussed the employed NH_3 emissions in detail.

ACPD
15, 29705–29745, 2015

A one-week episode of north-easterly winds during end of July corresponds in the time series plots to a strong decline in sNH_4 concentrations at Zingst and a strong increase at Westerland. The increase at Westerland is due to NH_3-rich air from Denmark. Although modeled concentrations increased considerably, measured concentrations increased even more. This result might be due to under-predicted emissions or over-predicted NH_3/NH_4^+ deposition. The discrepancy is not caused by sea salt. Remarkably, at Zingst, the modeled sNH_4 concentrations decreased, whereas the measured concentrations increased during this episode. No major landmasses are on the route between the Swedish coast and Zingst, the path by which the air masses likely travelled. If we consider the measured NH_3 and NH_4^+ concentrations individually (which one should not do, EMEP, 2014, Chp. 3), the measured sNH_4 consists primarily of NH_3 (> 95 % by mass, not shown here). Because NH_3 has a short atmospheric lifespan, we assume that most sNH_4 is transported over a short distance and does not originate from Sweden. The NH_3 may be emitted from the sea surface (Barrett, 1998; Paulot et al., 2015). Norman and Leck (2005) found oceanic emissions to be relevant contributors to atmospheric NH_3 in remote marine regions. These oceanic NH_3 emissions would explain the generally under-predicted concentrations at coastal stations. However, these emissions are approximately two to three orders of magnitude lower than land-based emissions. Additionally, a brief look on chlorophyll *a* data (Lavender et al., 2015) does not indicate the presence of algae blooms. Therefore, marine NH_3 cannot account for the entire difference at Zingst. Another reason might be incorrectly predicted wind directions caused by sea and land breezes and planetary boundary layer height (e.g. Miao et al., 2009). Sea and land breezes during day and night do not form in COSMO-CLM with the given setup, version and grid resolution (M. Schulz, personal communication, 2015). Furthermore, certain land-based NH_3 sources, which are located close to the measurement station, might not be considered by the employed emission dataset. This topic needs to be considered further.

Predicted and measured sNO_3 concentrations are not well correlated at Westerland in either seasons and at all stations in summer. Approximately half of the measure-

ACPD
15, 29705–29745, 2015

ments at Westerland were under the detection limit and not in the EMEP database. Thus, the peak concentrations were measured and compared. Comparing peak concentrations is biased because they are often over- or underestimated, e.g., via smoothing in the discretization. Therefore, an analysis of the sNO_3 Westerland data is problematic. Additionally, peaks arise in the model results that do not exist in the measurements. This effect may be due to the employed shipping emission inventory, which contains the weekly averaged shipping emissions of 2011 (whereas the model year is 2008) or due to problems with the measurements.

Im (2013), Liu et al. (2015) and Kelly et al. (2014) found that sea salt has a significant impact on atmospheric nitrate concentrations. In Im (2013) and Liu et al. (2015), particulate nitrate concentrations considerably increased when sea salt was added. They increased even more when surf zone emissions were activated (Im, 2013, Table 4). The emission and meteorological regimes in the Mediterranean and Pearl River Delta regions are different from those in the North Sea region, which may account for the different behavior. Due to high agricultural activity in the North Sea region, sufficient fine particles and ammonia are available for the condensation of ammonium nitrate onto existing particles. As described above, ammonium and nitrate concentrations correlate well in the model but are less correlated in reality. If the nitrate condensation is NH_3 limited in the Mediterranean region, modeled nitrate may condense on particles only in exchange for the release of HCl. According to the both other studies, HCl displacement is a relevant process in those regions. Hence, comparing the NH_3/NH_4^+ concentrations would be interesting. Additionally, Sahara dust is blown from the boundaries into the model domain of Im (2013). The dust may have an indirect effect on atmospheric chemistry that is not present in this study because desert dust is not included in this study's boundary conditions.

When sea salt emissions were deactivated, sNH_4 and sNO_3 concentrations increased and xSO_4 concentrations decreased. This observation is confusing because we expected xSO_4, NH_4^+ and NO_3^- concentrations to increase: the lack of sea salt results in fewer coarse particles, more condensation on fine particles and more nucle-

ACPD
15, 29705–29745, 2015

ation. Because fine particles are deposited more slowly than coarse ones, we expected the concentrations of condensing species to rise. Particulate sulfate does not evaporate back into the gas phase. Consequently, it remains adhered to coarse sea salt particles, which is why we expected an increase in sulfate in the zero case. The decreased sulfate concentrations may be due to decreased sulfate production by heterogeneous chemical reactions. In CMAQ, H_2SO_4 is formed from SO_2 via heterogeneous reactions on wet particle surfaces (Seinfeld and Pandis, 2006, Chp. 6.13) and by gas phase reactions. Deactivating sea salt emissions decreases the availability of wet particles considerably, therefore reducing heterogeneous H_2SO_4 production. This process is confirmed by increased production of H_2SO_4 in the gas phase and slightly higher SO_2 concentrations when sea salt emissions are deactivated, which can be found in the model output.

The impact of surf zone emissions on atmospheric sNH_4, sNO_3, and xSO_4 concentrations is negligible.

5 Conclusions

Measured sea salt concentrations are fairly well represented in the given model setup. Commonly, sea salt peak concentrations are overestimated. The current parameterization might overestimate sea salt emissions under strong wind conditions during the winter. This overestimation should be evaluated in future studies. A few peak concentrations are underestimated, indicating that one or more sea salt particle generation processes are not considered in the current sea salt emission parameterizations. These parameterizations should be tested with alternative sea salt emission source functions to determine whether these alternatives provide better predictions in these situations. However, the underestimated peak concentrations may be due to differences between the modeled meteorology and the real-world meteorology, as well. Figure 5 clearly shows that salinity-dependent scaling of sea salt emissions is important in marginal seas with salinities that differ from 35 ‰.

ACPD
15, 29705–29745, 2015

Surf zone emissions do not generally improve or deteriorate estimated sea salt concentrations in the presented model setup. Their effect on xSO_4, sNH_4, and sNO_3 is negligible. At a finer grid resolution, however, the impact of surf zone emissions might be relevant due to a relatively higher surf zone fraction. The general effect of sea salt particles on atmospheric xSO_4, sNH_4, and sNO_3 concentrations is low. The concentrations of sNH_4 and sNO_3 increased when sea salt emissions were deactivated, whereas xSO_4 concentrations decreased. The latter is expected to be caused by reduced H_2SO_4 production on particle surfaces. Im (2013); Liu et al. (2015) and Kelly et al. (2014) found that sea salt had a stronger impact on nitrate than found is this study. We assume that this difference is due to different emission and air pollution regimes, in particular due to NH_3 emissions. In one 10 day episode in late July, sNH_4 concentrations were considerably underestimated by the model. The reason for this is unclear. However, it is not related to sea salt particles.

For an improved validation it would be favorable to have hourly resolved measurements of these species and individual measurements of NO_3^-, HNO_3, NH_4^+, and NH_3 available. Data from both coastal and inland stations are needed in order to evaluate whether either the emission parameterization or modeled atmospheric transport processes lead to observed discrepancies. Size resolved sea salt measurements would be of high value for this process. Finally, more experimental work is needed in the subject of determining parameterizations for surf zone emissions.

The Supplement related to this article is available online at doi:10.5194/acpd-15-29705-2015-supplement.

Acknowledgements. Beate Geyer provided COSMO-CLM meteorology data which can be accessed via the Climate and Environmental Retrieval and Archive (CERA) of the German Climate Computing Centre (DKRZ). Salinity data were extracted from ECOSMO simulations. We thank Anna Backes, Matthias Karl and Markus Schultze from our institute for discussions on the model results. Additionally, Anna Backes provided GIS related data for this study.

ACPD
15, 29705–29745, 2015

Uma Shankar, James Kelly and Brett Gantt (US EPA) answered very detailed on questions on the inline sea salt emissions of CMAQ. A general thanks goes to the US EPA and the CMAQ development team for providing this high quality chemistry transport model as open source product. EMEP measurement data were extracted from the EBAS database which is maintained and further developed by the Norwegian Institute for Air Research (NILU). Statistical evaluation and most plotting were performed by R. Remaining plots were created with the Generic Mapping Tools (GMT) developed and maintained by Paul Wessel, Walter H. F. Smith, Remko Scharroo, Joaquim Luis and Florian Wobbe. Simulation data was processed with the Climate Data Operators (cdo) by Uwe Schultz-Weider from Max-Planck-Institute for Meteorology and with the netCDF Operators (NCO) by Charlie Zender and Henry Butowsky.

The article processing charges for this open-access publication were covered by a Research Centre of the Helmholtz Association.

References

Aulinger, A., Matthias, V., Zeretzke, M., Bieser, J., Quante, M., and Backes, A.: The impact of shipping emissions on air pollution in the Greater North Sea region – Part 1: Current emissions and concentrations, Atmos. Chem. Phys. Discuss., 15, 11277–11323, doi:10.5194/acpd-15-11277-2015, 2015. 29711

Backes, A., Aulinger, A., Bieser, J., Matthias, V., and Quante, M.: Ammonia Emissions In Europe, Part I: Development of a dynamical ammonia emissions inventory, Atmos. Environ., in revision, 2015a. 29710, 29722

Backes, A., Aulinger, A., Bieser, J., Matthias, V., and Quante, M.: Ammonia emissions in Europe, Part II: How ammonia emission abatement strategies affect secondary aerosols, Atmos. Environ., in revision, 2015b. 29710

Barrett, K.: Oceanic ammonia emissions in Europe and their transboundary fluxes, Atmos. Environ., 32, 381–391, doi:10.1016/S1352-2310(97)00279-3, 1998. 29723

Bieser, J., Aulinger, A., Matthias, V., Quante, M., and van der Gon, H. D.: Vertical emission profiles for Europe based on plume rise calculations, Environ. Pollut., 159, 2935–2946, doi:10.1016/j.envpol.2011.04.030, 2011. 29710

ACPD
15, 29705–29745, 2015

Binkowski, F. S. and Roselle, S. J.: Models-3 Community Multiscale Air Quality (CMAQ) model aerosol component 1. Model description, J. Geophys. Res.-Atmos., 108, 4183, doi:10.1029/2001JD001409, 2003. 29710

Bowyer, P. A., Woolf, D. K., and Monahan, E. C.: Temperature dependence of the charge and aerosol production associated with a breaking wave in a whitecap simulation tank, J. Geophys. Res.-Oceans, 95, 5313–5319, doi:10.1029/JC095iC04p05313, 1990. 29711

Cai, X., Ziemba, L. D., and Griffin, R. J.: Secondary aerosol formation from the oxidation of toluene by chlorine atoms, Atmos. Environ., 42, 7348–7359, doi:10.1016/j.atmosenv.2008.07.014, 2008. 29707

Chomka, M. and Petelski, T.: Sea spray emission over the coastal zone, J. Aerosol Sci., 28, 103–104, doi:10.1016/S0021-8502(97)85052-5, 1997. 29721

Crippa, M., Janssens-Maenhout, G., Dentener, F., Guizzardi, D., Sindelarova, K., Muntean, M., Van Dingenen, R., and Granier, C.: Forty years of improvements in European air quality: the role of EU policy–industry interplay, Atmos. Chem. Phys. Discuss., 15, 20245–20285, doi:10.5194/acpd-15-20245-2015, 2015. 29707

Crisp, T. A., Lerner, B. M., Williams, E. J., Quinn, P. K., Bates, T. S., and Bertram, T. H.: Observations of gas phase hydrochloric acid in the polluted marine boundary layer, J. Geophys. Res.-Atmos., 119, 6897–6915, doi:10.1002/2013JD020992, 2014. 29707

de Leeuw, G., Neele, F. P., Hill, M., Smith, M. H., and Vignati, E.: Production of sea spray aerosol in the surf zone, J. Geophys. Res.-Atmos., 105, 29397–29409, doi:10.1029/2000JD900549, 2000. 29720, 29721

EMEP: EMEP Manual for Sampling and Analysis, EMEP, available at: http://www.nilu.no/projects/ccc/manual/index.html (last access: 30 October 2015), 2014. 29714, 29723

Fountoukis, C. and Nenes, A.: ISORROPIA II: a computationally efficient thermodynamic equilibrium model for K^+–Ca^{2+}–Mg^{2+}–NH_4^+–Na^+–SO_4^{2-}–NO_3^-–Cl^-–H_2O aerosols, Atmos. Chem. Phys., 7, 4639–4659, doi:10.5194/acp-7-4639-2007, 2007. 29709

Fuentes, E., Coe, H., Green, D., de Leeuw, G., and McFiggans, G.: On the impacts of phytoplankton-derived organic matter on the properties of the primary marine aerosol – Part 1: Source fluxes, Atmos. Chem. Phys., 10, 9295–9317, doi:10.5194/acp-10-9295-2010, 2010. 29721

Gantt, B., Meskhidze, N., Facchini, M. C., Rinaldi, M., Ceburnis, D., and O'Dowd, C. D.: Wind speed dependent size-resolved parameterization for the organic mass fraction of sea spray

ACPD
15, 29705–29745, 2015

aerosol, Atmos. Chem. Phys., 11, 8777–8790, doi:10.5194/acp-11-8777-2011, 2011. 29707, 29711
Gathman, S. G. and Hoppel, W. A.: Surf electrification, J. Geophys. Res., 75, 4525–4529, doi:10.1029/JC075i024p04525, 1970. 29711
Geyer, B.: High-resolution atmospheric reconstruction for Europe 1948–2012: coastDat2, Earth Syst. Sci. Data, 6, 147–164, doi:10.5194/essd-6-147-2014, 2014. 29710
Geyer, B. and Rockel, B.: coastDat-2 COSMO-CLM Atmospheric Reconstruction, World Data Center for Climate (WDCC), Hamburg, Germany, doi:10.1594/WDCC/coastDat-2_COSMO-CLM, 2013. 29710
Gong, S. L.: A parameterization of sea-salt aerosol source function for sub- and super-micron particles, Global Biogeochem. Cy., 17, 1097, doi:10.1029/2003GB002079, 2003. 29708, 29711, 29712, 29720
Huijnen, V., Williams, J., van Weele, M., van Noije, T., Krol, M., Dentener, F., Segers, A., Houweling, S., Peters, W., de Laat, J., Boersma, F., Bergamaschi, P., van Velthoven, P., Le Sager, P., Eskes, H., Alkemade, F., Scheele, R., Nédélec, P., and Pätz, H.-W.: The global chemistry transport model TM5: description and evaluation of the tropospheric chemistry version 3.0, Geosci. Model Dev., 3, 445–473, doi:10.5194/gmd-3-445-2010, 2010. 29710
Im, U.: Impact of sea-salt emissions on the model performance and aerosol chemical composition and deposition in the East Mediterranean coastal regions, Atmos. Environ., 75, 329–340, doi:10.1016/j.atmosenv.2013.04.034, 2013. 29708, 29722, 29724, 29726
Jaeglé, L., Quinn, P. K., Bates, T. S., Alexander, B., and Lin, J.-T.: Global distribution of sea salt aerosols: new constraints from in situ and remote sensing observations, Atmos. Chem. Phys., 11, 3137–3157, doi:10.5194/acp-11-3137-2011, 2011. 29707, 29708
Kelly, J. T., Bhave, P. V., Nolte, C. G., Shankar, U., and Foley, K. M.: Simulating emission and chemical evolution of coarse sea-salt particles in the Community Multiscale Air Quality (CMAQ) model, Geosci. Model Dev., 3, 257–273, doi:10.5194/gmd-3-257-2010, 2010. 29711, 29712, 29713, 29722
Kelly, J. T., Baker, K. R., Nowak, J. B., Murphy, J. G., Markovic, M. Z., VandenBoer, T. C., Ellis, R. A., Neuman, J. A., Weber, R. J., Roberts, J. M., Veres, P. R., de Gouw, J. A., Beaver, M. R., Newman, S., and Misenis, C.: Fine-scale simulation of ammonium and nitrate over the South Coast Air Basin and San Joaquin Valley of California during CalNex-2010, J. Geophys. Res. Atmos., 119, 3600–3614, doi:10.1002/2013JD021290, 2014. 29722, 29724, 29726

ACPD
15, 29705–29745, 2015

Knipping, E. M. and Dabdub, D.: Impact of chlorine emissions from sea-salt aerosol on coastal urban ozone, Environ. Sci. Technol., 37, 275–284, doi:10.1021/es025793z, 2003. 29707
Lavender, S., Jackson, T., and Sathyendranath, S.: The Ocean Colour Climate Change Initiative – merging ocean colour observations seamlessly, Ocean Challenge, 21, 29–31, 2015. 29723
Lewis, E. R. and Schwartz, S. E.: Sea Salt Aerosol Production: Mechanisms, Methods, Measurements and Models – A Critical Review, vol. 152, AGU, Washington, D. C., doi:10.1029/GM152, 2004. 29711
Liu, Y., Zhang, S., Fan, Q., Wu, D., Chan, P., Wang, X., Fan, S., Feng, Y., and Hong, Y.: Accessing the Impact of Sea-Salt Emissions on Aerosol Chemical Formation and Deposition over Pearl River Delta, China, Aerosol Air Qual. Res., 15, 2232–2245, doi:10.4209/aaqr.2015.02.0127, 2015. 29708, 29724, 29726
Lövblad, G., Tarrasón, L., Tørseth, K., and Dutchak, S.: EMEP Assessment Part I – European Perspective, Tech. rep., Norwegian Meteorological Institute, Oslo, Norway, P. O. Box 43, N-313, 2004. 29707
Manders, A., Schaap, M., Querol, X., Albert, M., Vercauteren, J., Kuhlbusch, T., and Hoogerbrugge, R.: Sea salt concentrations across the European continent, Atmos. Environ., 44, 2434–2442, doi:10.1016/j.atmosenv.2010.03.028, 2010. 29708
Martensson, E. M., Nilsson, E. D., de Leeuw, G., Cohen, L. H., and Hansson, H.-C.: Laboratory simulations and parameterization of the primary marine aerosol production, J. Geophys. Res. Atmos., 108, 4297, doi:10.1029/2002JD002263, 2003. 29707, 29711, 29713, 29719, 29720
Miao, J.-F., Wyser, K., Chen, D., and Ritchie, H.: Impacts of boundary layer turbulence and land surface process parameterizations on simulated sea breeze characteristics, Ann. Geophys., 27, 2303–2320, doi:10.5194/angeo-27-2303-2009, 2009. 29723
Monahan, E. C. and Muircheartaigh, I. O.: Optimal power-law description of oceanic whitecap coverage dependence on wind speed, J. Phys. Oceanogr., 10, 2094–2099, doi:10.1175/1520-0485(1980)010<2094:OPLDOO>2.0.CO;2, 1980. 29708, 29711
Monahan, E. C., Davidson, K. L., and Spiel, D. E.: Whitecap aerosol productivity deduced from simulation tank measurements, J. Geophys. Res.-Oceans, 87, 8898–8904, doi:10.1029/JC087iC11p08898, 1982. 29711, 29712
Monahan, E. C., Spiel, D. E., and Davidson, K. L.: A Model of Marine Aerosol Generation via Whitecaps and Wave Disruption, Oceanographic Sciences Library, Springer, Dordrecht, the Netherlands, 167–174, 1986. 29708, 29712

ACPD
15, 29705–29745, 2015

Sensitivity of modeled atmospheric nitrogen species to variations in sea salt emissions

D. Neumann et al.

Norman, M. and Leck, C.: Distribution of marine boundary layer ammonia over the Atlantic and Indian Oceans during the Aerosols99 cruise, J. Geophys. Res.-Atmos., 110, D16302, doi:10.1029/2005JD005866, 2005. 29723

Otte, T. L. and Pleim, J. E.: The Meteorology-Chemistry Interface Processor (MCIP) for the CMAQ modeling system: updates through MCIPv3.4.1, Geosci. Model Dev., 3, 243–256, doi:10.5194/gmd-3-243-2010, 2010. 29710

Ovadnevaite, J., Manders, A., de Leeuw, G., Ceburnis, D., Monahan, C., Partanen, A.-I., Korhonen, H., and O'Dowd, C. D.: A sea spray aerosol flux parameterization encapsulating wave state, Atmos. Chem. Phys., 14, 1837–1852, doi:10.5194/acp-14-1837-2014, 2014. 29708

Paulot, F., Jacob, D. J., Johnson, M. T., Bell, T. G., Baker, A. R., Keene, W. C., Lima, I. D., Doney, S. C., and Stock, C. A.: Global oceanic emission of ammonia: constraints from seawater and atmospheric observations, Global Biogeochem. Cy., 29, 1165–1178, doi:10.1002/2015GB005106, 2015. 29723

Sarwar, G., Luecken, D., and Yarwood, G.: Chapter 2.9 Developing and implementing an updated chlorine chemistry into the community multiscale air quality model, in: Air Pollution Modeling and Its Application XVIII, edited by: Borrego, C. and Renner, E., vol. 6 of Developments in Environmental Science, 168–176, Elsevier, Amsterdam, the Netherlands, doi:10.1016/S1474-8177(07)06029-9, 2007. 29709

Schlünzen, K. H., and Sokhi, R. S.: Joint Report of COST Action 728 and GURME. Overview of Tools and Methods for Meteorological and Air Pollution Mesoscale Model Evaluation and User Training, WMO TD No 1457, WMO, Geneva, Switzerland, 2008. 29714

Seinfeld, J. H. and Pandis, S. N.: Atmospheric Chemistry and Physics: from Air Pollution to Climate Change, 2nd edn., Wiley-Interscience, Hoboken, New Jersey, USA, 2006. 29707, 29725

Spada, M., Jorba, O., Pérez García-Pando, C., Janjic, Z., and Baldasano, J. M.: Modeling and evaluation of the global sea-salt aerosol distribution: sensitivity to size-resolved and sea-surface temperature dependent emission schemes, Atmos. Chem. Phys., 13, 11735–11755, doi:10.5194/acp-13-11735-2013, 2013. 29708

Tanaka, P. L., Allen, D. T., McDonald-Buller, E. C., Chang, S., Kimura, Y., Mullins, C. B., Yarwood, G., and Neece, J. D.: Development of a chlorine mechanism for use in the carbon bond IV chemistry model, J. Geophys. Res.-Atmos., 108, 4145, doi:10.1029/2002JD002432, 2003. 29709

ACPD
15, 29705–29745, 2015

Sensitivity of modeled atmospheric nitrogen species to variations in sea salt emissions

D. Neumann et al.

Tian-Kunze, X., Kaleschke, L., Weller, R., König-Langlo, G., Wa- genbach, D., Rast, S., Santos, G., Richter, A., and Begoin, M.: Sea ice as a source of sea salt aerosol: A trajectory study of 25 years of year-round sea salt aerosol record at Neumayer, Antarctica, in: Geophysical Research Abstracts Vol. 11, EGU 2009, Vienna, Austria, p. 8934, 2009. 29722

Whitten, G. Z., Heo, G., Kimura, Y., McDonald-Buller, E., Allen, D. T., Carter, W. P., and Yarwood, G.: A new condensed toluene mechanism for Carbon Bond: CB05-TU, Atmos. Environ., 44, 5346–5355, doi:10.1016/j.atmosenv.2009.12.029, 2010. 29709

Yang, X., Pyle, J. A., and Cox, R. A.: Sea salt aerosol production and bromine release: Role of snow on sea ice, Geophys. Res. Lett., 35, L16815, doi:10.1029/2008GL034536, 2008. 29722

Yarwood, G., Rao, S., Yocke, M., and Whitten, G. Z.: Updates to the Carbon Bond Chemical Mechanism: CB05, Final report to project rt-04-00675, U. S. Environmental Protection Agency, Research Triangle Park, NC 27703, USA, 2005. 29709

Zhang, K. M., Knipping, E. M., Wexler, A. S., Bhave, P. V., and Tonnesen, G. S.: Size distribution of sea-salt emissions as a function of relative humidity, Atmos. Environ., 39, 3373–3379, doi:10.1016/j.atmosenv.2005.02.032, 2005. 29712

ACPD
15, 29705–29745, 2015

Table 1. Sea salt emission scenarios.

case	description
base	standard CMAQ emissions: 50 m surf zone, coast line from Natural Earth data set, linearly scaled with salinity
noSurf	like base but surf zone is treated like open ocean
zero	no sea salt

ACPD
15, 29705–29745, 2015

Table 2. Statistical values (R, NMB and MNB) for the comparison of measured and modeled (base and noSurf scenarios) sodium concentrations at three stations (DE0001R, DE0002R and DE0009R) and during two time periods (winter and summer 2008).

Na^+			R	MNB	RAE	n
win	base	DE1	0.76	1.01	1.89	60
	noSurf		0.75	0.65	1.84	60
	base	DE2	0.67	1.75	0.42	55
	noSurf		0.74	1.02	0.40	55
	base	DE9	0.79	1.24	0.72	60
	noSurf		0.82	0.69	0.64	60
sum	base	DE1	0.70	2.37	0.72	61
	noSurf		0.79	1.17	0.63	61
	base	DE2	0.70	−0.33	0.18	60
	noSurf		0.71	−0.43	0.20	60
	base	DE9	0.69	0.20	0.26	61
	noSurf		0.62	−0.16	0.31	61

ACPD
15, 29705–29745, 2015

Table 3. Similar to Table 2 but with the addition of xSO_4 (corrected sulfate) concentrations. Three sea salt emissions scenarios – base, noSurf, and zero – are considered.

xSO_4			R	MNB	RAE	n
win	base		0.67	0.17	0.22	58
	noSurf	DE1	0.67	0.17	0.22	58
	zero		0.66	0.17	0.22	58
	base		0.64	−0.15	0.55	54
	noSurf	DE2	0.63	−0.15	0.55	54
	zero		0.63	−0.15	0.55	54
	base		0.75	0.16	0.36	60
	noSurf	DE9	0.75	0.15	0.36	60
	zero		0.75	0.15	0.36	60
sum	base		0.73	−0.11	0.13	60
	noSurf	DE1	0.73	−0.11	0.13	60
	zero		0.71	−0.11	0.13	60
	base		0.57	0.12	0.21	60
	noSurf	DE2	0.57	0.11	0.21	60
	zero		0.58	0.08	0.20	60
	base		0.68	0.08	0.18	61
	noSurf	DE9	0.68	0.08	0.18	61
	zero		0.68	0.05	0.18	61

ACPD
15, 29705–29745, 2015

Table 4. Similar to Table 2 but with the addition of sNH_4 ($NH_3 + NH_4^+$) concentrations. Three sea salt emissions scenarios – base, noSurf, and zero – are considered.

sNH_4			R	MNB	RAE	n
win	base		0.60	−0.46	1.00	58
	noSurf	DE1	0.61	−0.45	0.99	58
	zero		0.60	−0.39	0.96	58
	base		0.59	0.25	1.28	54
	noSurf	DE2	0.59	0.26	1.28	54
	zero		0.59	0.31	1.31	54
	base		0.72	−0.19	0.81	57
	noSurf	DE9	0.72	−0.19	0.81	57
	zero		0.71	−0.12	0.77	57
sum	base		0.69	−0.57	1.29	61
	noSurf	DE1	0.69	−0.56	1.29	61
	zero		0.69	−0.55	1.27	61
	base		0.63	0.39	0.88	60
	noSurf	DE2	0.63	0.39	0.88	60
	zero		0.62	0.40	0.89	60
	base		0.46	−0.02	0.60	59
	noSurf	DE9	0.46	−0.01	0.60	59
	zero		0.47	0.00	0.60	59

ACPD
15, 29705–29745, 2015

Table 5. Similar to Table 2 but with the addition of sNO_3 ($HNO_3 + NO_3^-$) concentratios. Three sea salt emissions scenarios – base, noSurf, and zero – are considered.

sNO_3			R	MNB	RAE	n
win	base		0.10	1.17	0.76	21
	noSurf	DE1	0.10	1.19	0.76	21
	zero		0.11	1.48	0.81	21
	base		0.64	0.00	0.67	50
	noSurf	DE2	0.64	0.01	0.67	50
	zero		0.67	0.10	0.68	50
	base		0.76	−0.17	0.56	54
	noSurf	DE9	0.76	−0.16	0.57	54
	zero		0.77	−0.08	0.58	54
sum	base		−0.14	0.41	0.25	26
	noSurf	DE1	−0.14	0.43	0.26	26
	zero		−0.13	0.57	0.28	26
	base		0.34	0.05	0.31	59
	noSurf	DE2	0.34	0.06	0.31	59
	zero		0.34	0.16	0.32	59
	base		0.55	−0.23	0.26	56
	noSurf	DE9	0.55	−0.22	0.26	56
	zero		0.55	−0.14	0.26	56

ACPD
15, 29705–29745, 2015

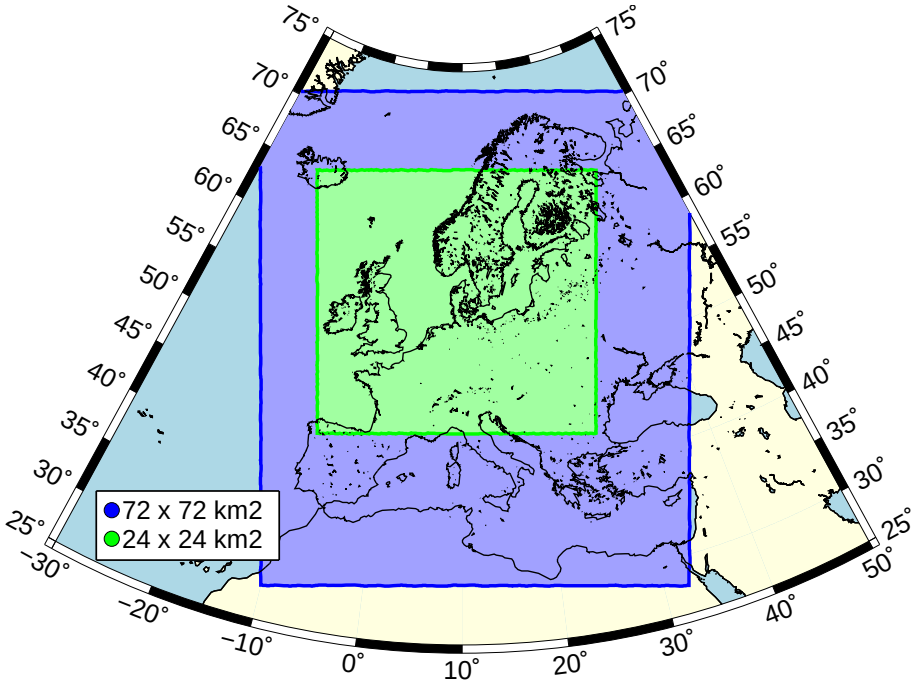

Figure 1. Study region and size of the model grids. The coarse grid (blue) includes Europe and parts of northern Africa. The first nested grid (green) includes Northwestern Europe, including the North and Baltic Seas.

ACPD
15, 29705–29745, 2015

Sensitivity of modeled atmospheric nitrogen species to variations in sea salt emissions

D. Neumann et al.

Figure 2. The EMEP stations chosen for the comparison to CMAQ data. Red circles indicate the stations discussed in Sect. 4. Data from the other stations are attached in the Supplement.

ACPD
15, 29705–29745, 2015

Sensitivity of modeled atmospheric nitrogen species to variations in sea salt emissions

D. Neumann et al.

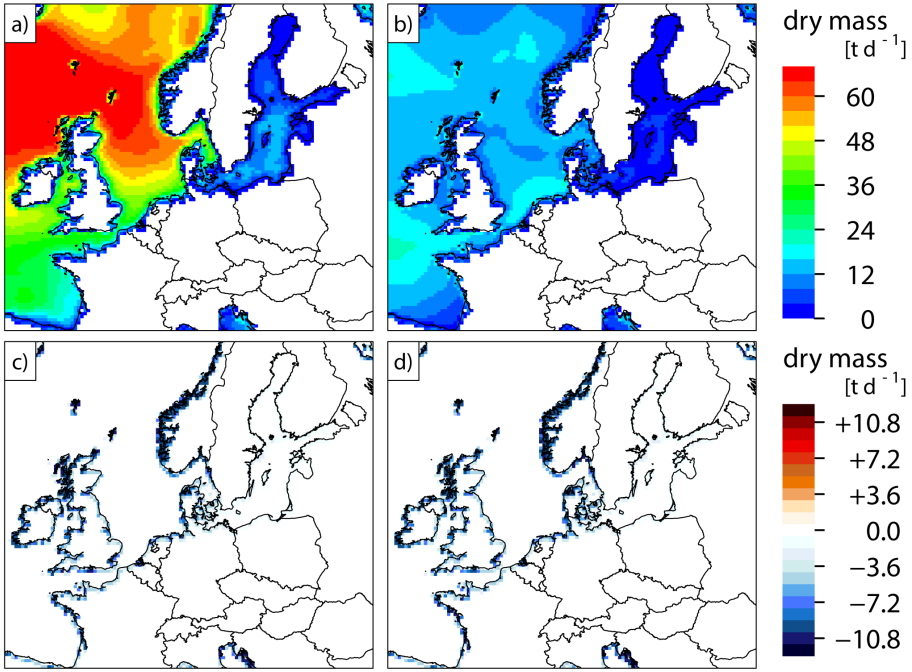

Figure 3. Average total sea salt emissions in t/d of the base case (top, **a** and **b**) in winter 2008 **(a)** and summer 2008 **(b)**. The difference noSurf – base case is shown in the bottom row (**c** and **d**).

ACPD
15, 29705–29745, 2015

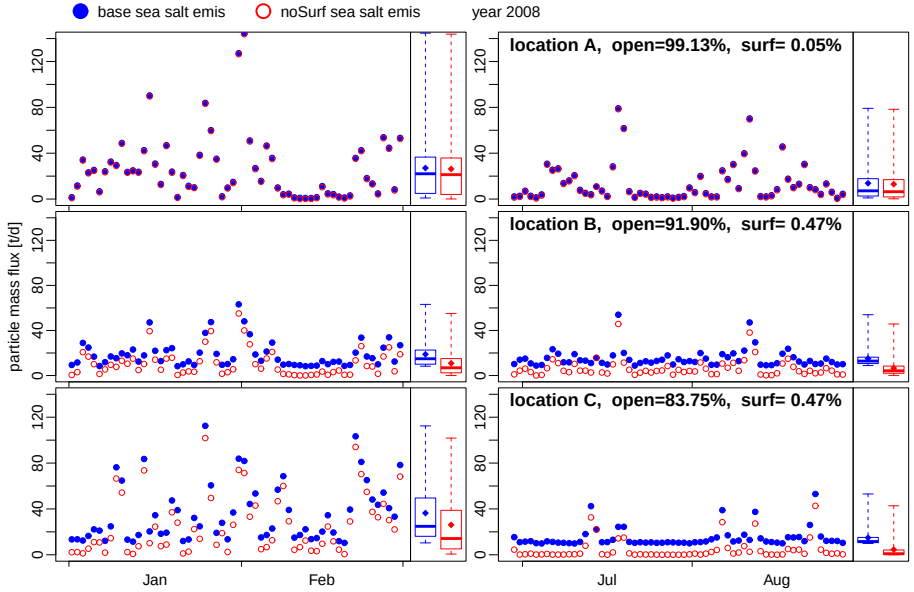

Figure 4. Daily averaged sea salt emission flux in t/d in three exemplary coastal grid cells (one per row) in winter 2008 (left) and summer 2008 (right). The fraction of open ocean and surf zone is listed in the plots on the right. The remaining share is land. Location A is located on the Dutch coast, location B is on the German coast and location C is on the Norwegian Atlantic coast.

ACPD
15, 29705–29745, 2015

Sensitivity of modeled atmospheric nitrogen species to variations in sea salt emissions

D. Neumann et al.

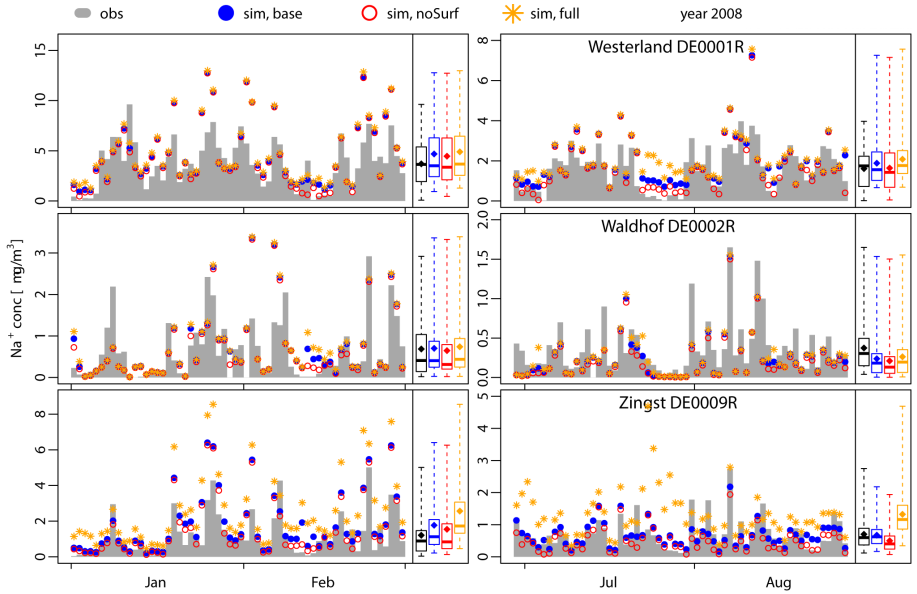

Figure 5. Measured (gray bars and black boxplots) and modeled (colored symbols) sodium concentrations at three stations (top to bottom) during winter 2007/08 (left) and summer 2008 (right). The orange line indicates sodium concentrations without salinity-dependent downscaling of sea salt emissions. On the left of each plot, the time series of the data are plotted. To the right of each time series, box plots showing minimum, 25 % percentile, median, 75 % percentile, maximum and mean values (rhombus) are shown.

ACPD
15, 29705–29745, 2015

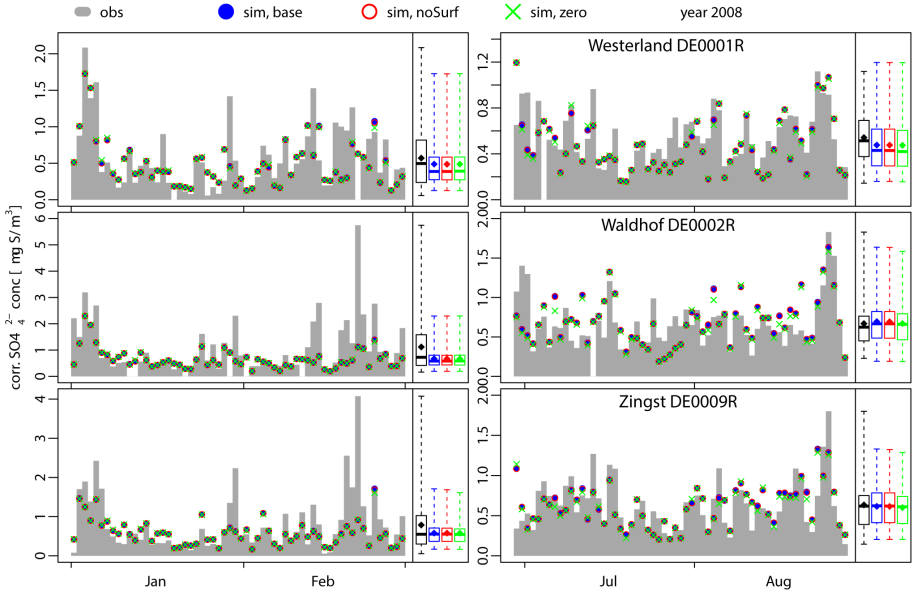

Figure 6. Similar to Fig. 5 but with the addition of xSO_4 values and showing base, noSurf, and zero sea salt emission cases.

ACPD
15, 29705–29745, 2015

Sensitivity of modeled atmospheric nitrogen species to variations in sea salt emissions

D. Neumann et al.

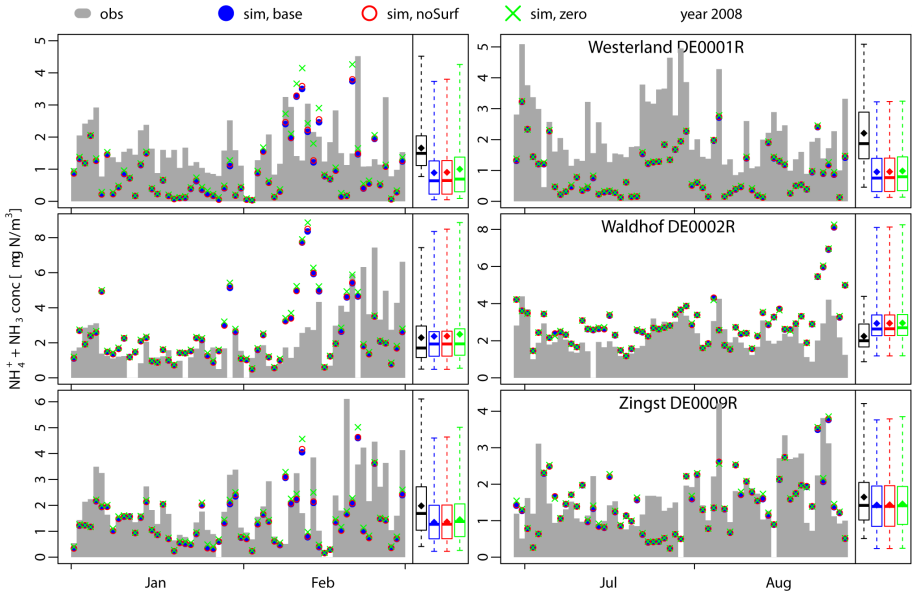

Figure 7. Similar to Fig. 6 but with the addition of sNH_4 values.

ACPD
15, 29705–29745, 2015

Sensitivity of modeled atmospheric nitrogen species to variations in sea salt emissions

D. Neumann et al.

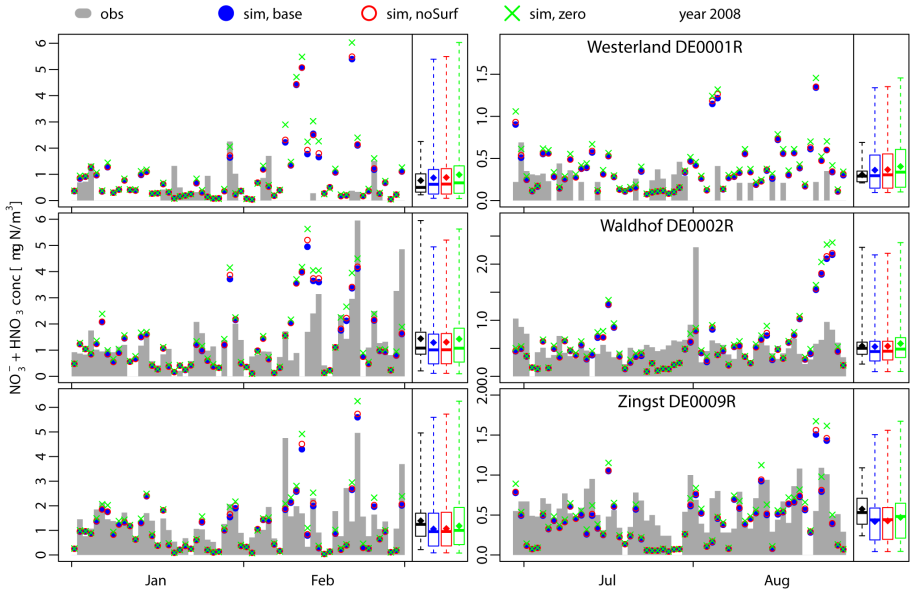

Figure 8. Similar to Fig. 6 but with addition of sNO_3 values.

ACPD
15, 29705–29745, 2015

Sensitivity of modeled atmospheric nitrogen species to variations in sea salt emissions

D. Neumann et al.